Effect of internal flow on the photophoresis of a micron-sized liquid droplet

Takafumi Iwaki*
Okayama Institute for Quantum Physics, Kyoyama 1-9-1, Okayama 700-0015, Japan
(Received 26 January 2010; revised manuscript received 30 April 2010; published 24 June 2010)

Light irradiation can induce the vectorial motion of an aerosol particle. This phenomenon is often explained in terms of inelastic collision between gas molecules and the aerosol particle under a temperature gradient. We considered the photophoresis of a micron-sized liquid droplet in a rarefied gas atmosphere based on the Boltzmann equation for the atmosphere coupled with the Navier-Stokes equation for the droplet. Two features attributable to induced internal flow in the droplet are analyzed: the contribution of homogeneous energy inflow to the motion of the droplet and the nonlinear scaling of the photophoretic velocity depending on the irradiated light intensity.

DOI: 10.1103/PhysRevE.81.066315 PACS number(s): 47.61.−k, 92.60.Mt, 47.15.G−, 05.70.Np

I. INTRODUCTION

The behavior of a fluid system depends on its temperature. In the presence of a local temperature distribution, a fluid system is called a thermofluid system. The most characteristic phenomenon seen in such a thermofluid system is the mass flow induced by a temperature gradient. Within the framework of classical fluid dynamics, a temperature gradient induces mass flow only when it couples with other forces through a density variation, such a gravitational convection. On the other hand, for a long time we have also been aware of thermally driven mass flow beyond the above criterion. For example, Marangoni convection arising from a temperature- or surfactant-dependent surface tension has interested many researchers in the field of nonlinear nonequilibrium physics [1–3].

For gas on a surface with a temperature gradient, we encounter another classical example of such flow. The most famous example is a radiometer, and similar phenomena are widely known and have been studied for a long time. For example, under light irradiation, colloidal particles migrate [4–10]. This phenomenon is called photophoresis and was first recognized by Ehrenhaft in the early 20th century [4]. Today, photophoresis is studied from various perspectives; e.g., to understand astrophysical (geophysical) processes in the atmosphere [11,12], as a means of molecular segregation [13,14], to sort particles in conjunction with Brownian potential ratcheting [15], and for use in engineering applications [11,16].

In principle, the photophoretic force arises from two mechanisms. When an electromagnetic wave is scattered by a colloidal particle, momentum is transferred between the wave and the particle to preserve the total momentum of the system. The force arising from this transfer is called photon pressure or scattering force and can be calculated from the ray optics [17] or directly from the Mie scattering solution [18]. If the particle is not transparent, a radiation distribution within the particle serves as a heat source through light absorption, which results in a temperature gradient on the particle surface. In this case, the momentum transfer between gas molecules and the photophoretic particle through molecular collisions becomes asymmetric with regard to the particle surface, and gas flow is induced [19]. The force arising from this mechanism is sometimes called the ΔT force [11].

In many cases, the photophoretic force applied to aerosol particles in a laboratory environment is considered to be mainly composed of the ΔT force [20]. In this case, photophoresis is essentially equivalent to thermophoresis, in which a temperature gradient of the ambient gas induces motion of the particle. Thus, photophoresis is often discussed in the same context as thermophoresis [21–23]. In the present paper, we focused on this case.

Even if an analysis of photophoresis is limited to the ΔT force, the exact physics of photophoresis are not simple. First, to derive a function for the heat source [24,25], we must solve a scattering problem for the electromagnetic wave. For a long time, the only analytical solution available was for a spherical particle [26,27]. Recently, however a nonspherical case [28–31] has been discussed, partly with the help of computers. If the particle is volatile, the effect of mass outflow due to evaporation should be considered [21,23,32]. Furthermore, the effect of blackbody radiation has sometimes been taken into account [23,32].

The most essential component of the ΔT force should be the detailed distribution of gas molecules around the particle (i.e., a solution for a fluid equation) and the interaction at the interface (i.e., a boundary condition). Since momentum transfer is essential in this phenomenon, a model equation must include the velocity distribution. Consequently, the Boltzmann equation with a kinetic boundary condition has been studied as a model equation for describing photophoretic or thermophoretic phenomena. Although kinetic boundary conditions are derived, to a certain degree, from a microscopic perspective, the true nature of the kinetics at the interface is not actually known. The most frequently used kinetic boundary condition for a particle-gas interface is called the Maxwell-type boundary condition, which is a linear combination of specular reflection, where individual molecules are reflected completely elastically, and diffuse reflection, where the reflected molecules follow a Maxwellian distribution according to the surface temperature. The weight

*Present address: Fukui Institute for Fundamental Chemistry, Kyoto University, Takano-Saikai-Cho 34-4, Kyoto 606-8103, Japan.

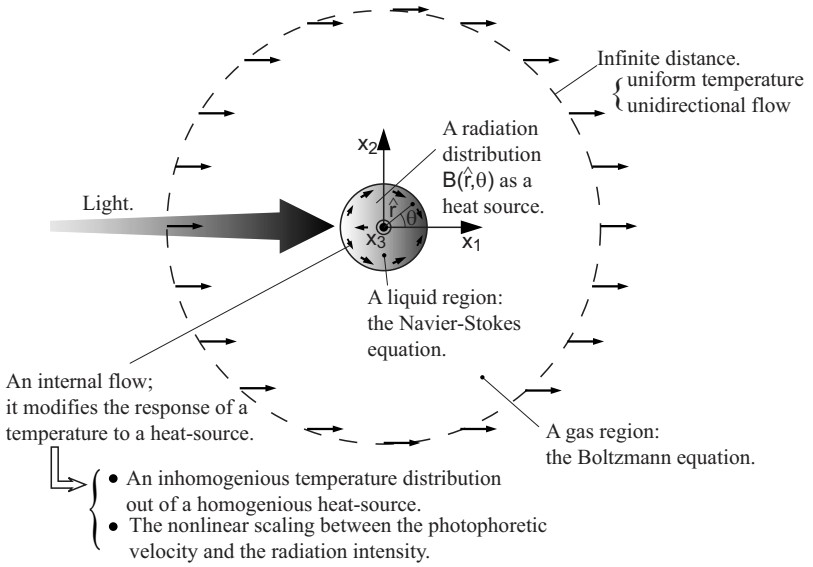

FIG. 1. A schematic representation of the problem considered in the present paper. According to the size and the complex refraction index of a photophoretic particle, photophoresis occurs in the positive and negative directions. While this figure corresponds to the negative photophoresis, we do not focus on a particular irradiation problem, but consider response to a general distribution of radiation within a droplet.

of this diffuse reflection is called an accommodation coefficient.

The Boltzmann equation has been analyzed for two limiting cases with regard to the Knudsen number (Kn) which is the ratio of the mean free path ℓ_0 to the reference length scale L. One case is a free-molecule regime ($\mathrm{Kn}\to\infty$), where interactions between gas molecules can be omitted as a matter of fact [23,25,32]. In the case of thermophoresis, the thermophoretic force does not greatly depend on the accommodation coefficients [33]. In 1972, Phillips [34] considered the case in which an accommodation coefficient in the tangential direction α_t and that in the normal direction α_n have separate values. He found that the thermophoretic force in the free-molecule limit is in proportion to $1+(\alpha_t-\alpha_n)/2$. Experimentally, in most gas-solid interfaces, α_t is close to unity and there is no inconsistency for α_n close to unity, though we do not know much about α_n [35]. This universality regarding accommodation coefficients is only applicable to a thermophoretic force. In photophoresis, a specular reflection produces no photophoretic force. The mean free path under atmospheric pressure is about several tens of nanometers. The free-molecule solution is applicable to nanometer- to micrometer-sized particles in a medium- to high-vacuum environment.

The other case is a continuum regime ($\mathrm{Kn}\to 0$), where the velocity distribution is rapidly relaxed and the gas, except for that in the vicinity of the particle, obeys the classical fluid equation. In this case, the problem can be reduced to solving the Navier-Stokes equations with slip boundary conditions [21,22,25,29,30]. This asymptotic treatment was first reported [36] before the quest for the free-molecule solution, but it took a long time to identify the complete set of first-order slip boundary conditions [37]. This perturbation approach has been extended to the third-order using the Boltzmann-Krook-Welander (BKW) model for a collision term by Sone and Aoki [38]. Although these results are only valid in the regime of small Knudsen numbers, it has been shown that Brock's formula for the thermophoretic force [37] acceptably agrees with the experimental data throughout the entire region of Knudsen numbers when the best data are used for the slip coefficients [35,39]. As a more rigorous approach, the intermediate region has recently been analyzed with a numerical solution for the linearized Boltzmann equation [40–43].

A more detailed history of the Boltzmann equation is available elsewhere [35]. A few experiments have been conducted on the thermophoresis or photophoresis of organic droplets [44,45]. However, so far, theoretical studies of thermophoresis or photophoresis have only treated the situation where there is no internal flow in the colloidal object or the effect of internal flow is negligible. One reason for this lack of interest is that most experimental studies have measured the force applied to an object at rest. In this case, the main contribution to an internal flow, i.e., the drag force due to air flow, is restricted. In addition, when the internal flow remains slow, the temperature distribution of the object is almost determined by the diffusion equation, and the influence of the flow velocity field is negligible. A few experimental studies measuring the dependence on the radiation intensity [20] have focused on the situation in which the photophoretic force or velocity linearly scales with the radiation power (the region of weak power), which may be another reason for the lack of a theoretical work on the effect of internal flow.

However, the effect of internal flow is a more interesting problem from a physical viewpoint. When internal flow is considered, two significant effects are expected. One is the occurrence of migration induced by homogeneous energy influx, and the other is the nonlinear scaling relationship between the photophoretic velocity and the magnitude of the energy influx. In the present paper, we analyze the photophoresis of a spherical micron-sized droplet based on the Boltzmann equation for a gas region coupled with the Navier-Stokes equation for the droplet and examine how the above two effects occur. Figure 1 shows a schematic representation of the considered problem. In Sec. II, we introduce an asymptotic solution of the Boltzmann equation for a spherical system, based on a discussion in a textbook [19], with a slight extension to the case where a spherical boundary surface has a flow field. In Sec. III, we summarize the theoretical formulation of the photophoretic problem of a

solid sphere based on the above asymptotic solution. In Sec. IV, we couple the Navier-Stokes equation with the Boltzmann equation and consider the slow velocity limit of the internal flow. Finally, in Sec. V, we analyze this system for a wide range of velocities with the aid of a numerical calculation, and discuss the physical properties of photophoresis that are characteristic to a droplet with internal flow.

II. BOLTZMANN EQUATION FOR A SPHERICAL SYSTEM

We consider a gas of identical molecules interacting through a spherical potential. In the coarse-grained model, the state of gas is represented by the time-dependent local ensemble of velocities $f(\boldsymbol{X},\boldsymbol{\xi},t)$, where $\boldsymbol{X}$ is a position vector, $\boldsymbol{\xi}$ is a velocity vector, and the distribution function is normalized to satisfy $\rho=\int f(\boldsymbol{X},\boldsymbol{\xi},t)d\xi$, where ρ is a local mass density of the gas. Unless the interaction between particles is long range or the density of the gas is too high, the time evolution of the velocity distribution function $f(\boldsymbol{X},\boldsymbol{\xi},t)$ is determined by the Boltzmann equation:

$$\partial_t f + \boldsymbol{\xi}\cdot\nabla_X f + \nabla_\xi(\boldsymbol{F}f) = J(f,f), \tag{1}$$

where ∇_X and ∇_ξ are, respectively, the divergence with respect to the position vector and the velocity vector, $\boldsymbol{F}$ is an external force, and $J(f,f)$ is the collision term that depends on the molecular model.

Usually, the Boltzmann equation is solved around some objects. When there is no mass flux across the boundaries of these objects, the Maxwell-type condition is widely used as the boundary condition for the objects.

$$f(\boldsymbol{X},\boldsymbol{\xi},t) = (1-\alpha)f\{\boldsymbol{X},\boldsymbol{\xi}-2[(\boldsymbol{\xi}-\boldsymbol{v}_w)\cdot\boldsymbol{n}]\boldsymbol{n},t\} + \frac{\alpha\sigma_w}{(2\pi RT_w)^{3/2}} \times\exp\left(-\frac{|\boldsymbol{\xi}-\boldsymbol{v}_w|^2}{2RT_w}\right) \quad [(\boldsymbol{\xi}-\boldsymbol{v}_w)\cdot\boldsymbol{n}>0], \tag{2}$$

$$\sigma_w = -\left(\frac{2\pi}{RT_w}\right)^{1/2}\int_{(\boldsymbol{\xi}-\boldsymbol{v}_w)\cdot\boldsymbol{n}<0}(\boldsymbol{\xi}-\boldsymbol{v}_w)\cdot\boldsymbol{n}f(\boldsymbol{X},\boldsymbol{\xi},t)d\boldsymbol{\xi}, \tag{3}$$

where T_w and $\boldsymbol{v}_w$ are the temperature and velocity of the boundary, respectively, and $\boldsymbol{n}$ is the unit vector normal to the boundary with a direction from the solid to the gas. The accommodation coefficient α varies from 0 to 1. The case $\alpha=1$ is called the diffuse-reflection condition, and this part in the Maxwell-type condition is the origin of the radiometric effect (thermophoresis).

The Boltzmann equation expresses a generalized conservation law, which includes classical hydrodynamic equations. Macroscopic variables used in classical hydrodynamics are defined as follows:

$$v_i = \frac{1}{\rho}\int \xi_i f(\boldsymbol{X},\boldsymbol{\xi},t)d\boldsymbol{\xi}, \tag{4}$$

$$3RT = \frac{1}{\rho}\int (\xi_i - v_i)^2 f(\boldsymbol{X},\boldsymbol{\xi},t)d\boldsymbol{\xi}, \tag{5}$$

$$p_{ij} = \int (\xi_i - v_i)(\xi_j - v_j)f(\boldsymbol{X},\boldsymbol{\xi},t)d\boldsymbol{\xi}, \tag{6}$$

$$q_i = \int \frac{1}{2}(\xi_i - v_i)(\xi_j - v_j)^2 f(\boldsymbol{X},\boldsymbol{\xi},t)d\boldsymbol{\xi}, \tag{7}$$

where R is the specific gas constant, T is the temperature, p_{ij} is the stress tensor, and q_i is heat-flow.

We now consider the case where the system is not far from the uniform Maxwell distribution f_0 with no flow;

$$f_0 = \frac{\rho_0}{(2\pi RT_0)^{3/2}}\exp\left(-\frac{\xi_i^2}{2RT_0}\right), \tag{8}$$

where ρ_0 is the reference density and T_0 is the reference temperature. The reference pressure p_0 is given from the definition as $p_0=p_{ii}/3=R\rho_0T_0$. When we introduce a reference length scale L and a reference time scale t_0, we obtain the following nondimensional variables:

$$x_i = X_i/L, \tag{9}$$

$$\hat{t} = t/t_0, \tag{10}$$

$$\zeta_i = \xi_i/\sqrt{2RT_0}, \tag{11}$$

$$\phi = f/f_0 - 1, \tag{12}$$

$$w = \rho/\rho_0 - 1, \tag{13}$$

$$u_i = v_i/\sqrt{2RT_0}, \tag{14}$$

$$\tau = T/T_0 - 1, \tag{15}$$

$$P_{ij} = p_{ij}/p_0 - \delta_{ij}, \tag{16}$$

$$Q_i = q_i/(p_0\sqrt{2RT_0}), \tag{17}$$

where δ_{ij} is the Kronecker delta.

Since $\phi\ll 1$, the Boltzmann equation (without external force) may be approximated by the following linearized form:

$$\mathrm{Sh}\frac{\partial\phi}{\partial\hat{t}} + \zeta_i\frac{\partial\phi}{\partial x_i}\phi = \frac{1}{k}\mathcal{L}(\phi), \tag{18}$$

where $\mathrm{Sh}=L/(t_0\sqrt{2RT_0})$ is called the Strouhal number and $k=\sqrt{\pi}\ell_0/(2L)$, where ℓ_0 is the mean free path of the gas in the equilibrium state, is the Knudsen number Kn multiplied by $\sqrt{\pi}/2$. Hereafter, we also call the number k the Knudsen number. The collision term $\mathcal{L}(\phi)$ is the linear part of the normalized $J(f,f)$ in Eq. (1). For simplicity, we adopt the BKW model equation, for which the linearized expression is

$$\mathcal{L}(\phi) = -\phi + w + 2\zeta_i u_i + \left(\zeta_i^2 - \frac{3}{2}\right)\tau. \tag{19}$$

On the boundary, the modified diffuse-reflection condition according to linearization is

$$\phi = \breve{\sigma}_w + 2\boldsymbol{\zeta}\cdot\boldsymbol{u}_w + \left(|\zeta|^2 - \frac{3}{2}\right)\tau_w \quad [(\boldsymbol{\zeta}-\boldsymbol{u}_w)\cdot\boldsymbol{n}>0], \tag{20}$$

$$\breve{\sigma}_w = \sqrt{\pi}\boldsymbol{u}_w \cdot \boldsymbol{n} - \frac{1}{2}\tau_w - 2\sqrt{\pi}\int_{(\boldsymbol{\zeta}-\boldsymbol{u}_w)\cdot\boldsymbol{n}<0} \boldsymbol{\zeta}\cdot\boldsymbol{n}\,\phi E d\boldsymbol{\zeta}. \quad (21)$$

The macroscopic variables are obtained in the following linearized form:

$$w = \int \phi E d\boldsymbol{\zeta}, \quad (22)$$

$$u_i = \int \zeta_i \phi E d\boldsymbol{\zeta}, \quad (23)$$

$$\frac{3}{2}\tau = \int \left(\zeta^2 - \frac{3}{2}\right)\phi E d\boldsymbol{\zeta}, \quad (24)$$

$$P_{ij} = 2\int \zeta_i\zeta_j \phi E d\boldsymbol{\zeta}, \quad (25)$$

$$Q_i = \int \zeta_i\zeta^2 \phi E d\boldsymbol{\zeta} - \frac{5}{2}u_i. \quad (26)$$

Linearization of the macroscopic variables is not always required because once ϕ is given, all macroscopic variables can be calculated in a straightforward manner. From a practical standpoint, however, the linearization of macroscopic variables is consistent and offers a good approximation as long as the linearized Boltzmann equation works well.

To obtain an analytical solution for a steady state, two approximation methods are known for two limiting cases where the Knudsen number k is much less than 1 and much greater than 1, respectively. As described above, the Knudsen number k is the ratio of the mean free path ℓ_0 to the reference length L. The mean free path of air molecules at room temperature at 1 atmosphere is 0.067 μm. For a micrometer-sized particle, k is below 0.1, and this situation corresponds to the case where $k \ll 1$. In this case, an asymptotic solution can be obtained as the sum of the Grad-Hilbert expansion [46] and the Knudsen-layer correction [19]. In the Grad-Hilbert expansion, a moderately varying solution ϕ_G can be written as a power series of k;

$$\phi_G = \phi_{G0} + \phi_{G1}k + \phi_{G2}k^2 + \cdots. \quad (27)$$

According to the order of k, the linearized Boltzmann equation is split into a series of integral equations:

$$\mathcal{L}(\phi_{G0}) = 0, \quad (28)$$

$$\mathcal{L}(\phi_{Gm}) = \zeta_i \frac{\partial \phi_{Gm-1}}{\partial x_i}. \quad (29)$$

According to the Grad-Hilbert expansion of the velocity distribution function, macroscopic variables can be written in a similar expansion form. A series of partial differential equations for these macroscopic variables is then derived from the above equations.

For the Knudsen-layer correction, a solution ϕ_K is considered, which varies rapidly in the direction of the normal vector on the boundary. This additional term is introduced to complement the Grad-Hilbert solution to satisfy the Maxwell-type boundary condition. If we introduce Knudsen-layer variables (η, χ_1, χ_2) as

$$x_i = k\eta n_i(\chi_1,\chi_2) + x_{wi}(\chi_1,\chi_2), \quad (30)$$

where n_i is the normal vector and x_{wi} represents the boundary surface. For ϕ_K, the linearized Boltzmann equation is split into the following series:

$$\mathcal{L}(\phi_{K0}) = \zeta_i n_i \frac{\partial \phi_{K0}}{\partial \eta}, \quad (31)$$

$$\mathcal{L}(\phi_{Km}) = \zeta_i n_i \frac{\partial \phi_{Km}}{\partial \eta} + \zeta_i \left(\frac{\partial \chi_a}{\partial x_i}\right)_0 \frac{\partial \phi_{Km-1}}{\partial \chi_a}, \quad (32)$$

where the parentheses $(\,)_0$ indicate that the enclosed quantity is evaluated at $\eta = 0$.

While the asymptotic analysis explained above can be performed in a straightforward manner, the actual calculation procedure (see, e.g., Sone [19]) is slightly complicated. In the linearized equation, the superposition principle of the solution holds true. Thus, we can treat an arbitrary problem as a combination of several elementary problems. In the present paper, we consider the gas around a spherical object, which can be reduced to the following elementary problems. The Cartesian coordinates and spherical coordinates are related as $(x_1,x_2,x_3) = (r\cos\theta, r\sin\theta\cos\varphi, r\sin\theta\sin\varphi)$.

Problem 1: the surface of the object has a homogeneous temperature $\tau_w = 0$ and no velocity $\boldsymbol{u}_w = 0$. At infinity, the gas has a flow velocity $\boldsymbol{u} = (1,0,0)$, with a homogeneous density $w = 0$ and a homogeneous temperature $\tau = 0$.

Problem 2: the surface of the object has a temperature gradient $\tau_w = \cos\theta$ but has no velocity $\boldsymbol{u}_w = 0$. At infinity, the gas is at rest $[\boldsymbol{u} = (0,0,0)]$ with a homogeneous density $w = 0$ and a homogeneous temperature $\tau = 0$.

Problem 3: the spherical object has internal flow. The flow velocity on the surface is given by $u_{wr} = 0$, $u_{w\theta} = \sin\theta$, and $u_{w\varphi} = 0$. The temperature of the surface is homogeneous $\tau_w = 0$. At infinity, the gas is at rest $[\boldsymbol{u} = (0,0,0)]$ with a homogeneous density $w = 0$ and a homogeneous temperature $\tau = 0$.

Here, we describe the solution of the linearized Boltzmann equation for problem 1 as ϕ_d, that for problem 2 as ϕ_1, and that for problem 3 as ϕ_v. Macroscopic variables corresponding to each solution are distinguished by superscript (d), (1), and (v), respectively. For the linearized Boltzmann equation, these boundary problems are introduced only for convenience because the deviation from the equilibrium state in the solution of ϕ is too large to justify linearization for these boundary values. In the actual analysis, we consider the case where the boundary values are multiplied by small quantities.

The solutions for problems 1 and 2 up to the third-order term are found in the textbook [19]. It is numerically known that these solutions are applicable to, at least, the range of the Knudsen number k from 0 to about 0.1. Macroscopic variables that are related to our problem are the total force acting on the spherical object $F_1 (F_2 = F_3 = 0)$, the $r-\theta$ component of

the stress tensor $P_{r\theta}$ on the boundary surface, and the heat flow across the surface of the object Q_r. These can be summarized as follows:

$$\frac{F_1^{(d)}}{p_0 L^2} = \bar{F}_1^{(d)} = 6\pi\gamma_1 k\left(1 + k_0 k - \frac{4}{3}A_d k^2 + \cdots\right), \tag{33}$$

$$\frac{P_{r\theta}^{(d)}}{\sin\theta} = \bar{P}_{r\theta}^{(d)} = \frac{3}{2}\gamma_1 k + \frac{9}{2}\gamma_1 k_0 k^2 + \cdots, \tag{34}$$

$$\frac{Q_r^{(d)}}{\cos\theta} = \bar{Q}_r^{(d)} = \left(\frac{3}{2}\gamma_3 + 3\int_\infty^0 H_A(\eta_0)d\eta_0\right)k^2 + \cdots, \tag{35}$$

$$\frac{F_1^{(1)}}{p_0 L^2} = \bar{F}_1^{(1)} = 4\pi\gamma_1(K_1 k^2 - 2A_t k^3 + \cdots), \tag{36}$$

$$\frac{P_{r\theta}^{(1)}}{\sin\theta} = \bar{P}_{r\theta}^{(1)} = 3k^2\left\{\gamma_1 K_1 + \gamma_3 - \int_\infty^0 [\Omega_1(\eta_0) + \Theta_1(\eta_0)]d\eta_0\right\} + \cdots, \tag{37}$$

$$\frac{Q_r^{(1)}}{\cos\theta} = \bar{Q}_r^{(1)} = \frac{5}{2}\gamma_2 k - \left(5\gamma_2 d_1 - 2\int_\infty^0 H_B(\eta_0)d\eta_0\right)k^2 + \cdots. \tag{38}$$

For problem 3, we obtain the following solution:

$$\frac{u_r^{(v)}}{\cos\theta} = -\frac{1}{r} + \frac{1}{r^3} + 3k_0\left(-\frac{1}{r} + \frac{1}{r^3}\right)k + \left[4\left(\frac{A_d - b_1}{r} + \frac{B_d - b_1}{r^3}\right) - 10\int_\infty^\eta Y_0(\eta_0)d\eta_0\right]k^2 + \cdots,$$

$$\frac{u_\theta^{(v)}}{\sin\theta} = \frac{1}{2}\left(\frac{1}{r} + \frac{1}{r^3}\right) + \frac{3}{2}\left[k_0\left(\frac{1}{r} + \frac{1}{r^3}\right) + 2Y_0(\eta)\right]k - 2\left[\frac{A_d - b_1}{r} - \frac{B_d - b_1}{r^3} - Y_d(\eta)\right]k^2 + \cdots,$$

$$\frac{\tau^{(v)}}{\cos\theta} = 20\left(\frac{d_4}{r^2} + \Theta_4(\eta)\right)k^2 + \cdots,$$

$$\frac{w^{(v)}}{\cos\theta} = -\frac{\gamma_1 k}{r^2} + \left(-(3\gamma_1 k_0 + 20d_4)\frac{1}{\hat{r}^2} + 20\Omega_4(\eta)\right)k^2 + \cdots,$$

where $\eta=(r-1)/k$. On the boundary, the force, the stress tensor and the heat flow are given as follows:

$$\frac{F_1^{(v)}}{p_0 L^2} = \bar{F}_1^{(v)} = 4\pi\gamma_1 k[1 + 3k_0 k - 4(A_d - b_1)k^2 + \cdots], \tag{39}$$

$$\frac{P_{r\theta}^{(v)}}{\sin\theta} = \bar{P}_{r\theta}^{(v)} = 3\gamma_1 k + 9\gamma_1 k_0 k^2 + \cdots, \tag{40}$$

TABLE I. The values of the total force (divided by $p_0 L^2$) $\bar{F}_1$, the $r-\theta$ component of the stress tensor (divided by $\sin\theta$) $\bar{P}_{r\theta}$, and the r component of the heat flow (divided by $\cos\theta$) $\bar{Q}_r$ for the BKW equation, in which we use the Knudsen number (times $\sqrt{\pi}/2$) $k=0.156\ 249\ 2$ for the force and stress tensor, and $k=0.192\ 228\ 4$ for the heat flow, to resemble [19] a hard-sphere gas of $k=0.1$. The scripts (d), (1), and (v) indicate the boundary conditions, which are explained in the body text.

	(d)	(1)	(v)
$\bar{F}_1$	2.51354	−0.11286	1.12251
$\bar{P}_{r\theta}$	0.12273	0.03662	0.24546
$\bar{Q}_r$	0.04248	0.20917	−0.00622

$$\frac{Q_r^{(v)}}{\cos\theta} = \bar{Q}_r^{(v)} = \left(\gamma_3 + 10\int_\infty^0 H_A(\eta_0)d\eta_0\right)k^2 + \cdots. \tag{41}$$

The coefficients γ_1, γ_2, γ_3, k_0, b_1, d_1, d_4, A_d, B_d, A_t, and K_1 and the Knudsen-layer functions $Y_0(\eta)$, $Y_d(\eta)$, $H_A(\eta)$, $H_B(\eta)$, $\Theta_1(\eta)$, $\Theta_4(\eta)$, $\Omega_1(\eta)$, and $\Omega_4(\eta)$ were introduced in the textbook [19]. The actual values of F_1, $P_{r\theta}$, and Q_r for each Problem are summarized in Table I for the case where $k=0.1$.

III. PHOTOPHORESIS OF A SOLID SPHERE

Before we consider the photophoresis of a spherical droplet, we briefly discuss the photophoresis of a solid sphere in terms of the linearized Boltzmann equation. The velocity distribution function of the gas around a solid sphere is given by

$$\phi = \bar{u}\phi_d + \bar{\tau}_w\phi_1, \tag{42}$$

where $\bar{u}=U(2RT_0)^{-1/2}$ is a nondimensional air-flow velocity at infinity, and $\bar{\tau}_w$ is the magnitude of the temperature gradient on the solid surface. When the temperature distribution of the solid object is denoted as $\tau_p=\Sigma_n\tau_{p,n}(r)P_n(\cos\theta)$, where $P_n(x)$ is a Legendre polynomial,

$$\bar{\tau}_w = \tau_{p,1}(1). \tag{43}$$

In the steady state, the migration velocity of the solid sphere $-\bar{u}$ and the temperature gradient on the sphere $\bar{\tau}_w$ are determined by the balance of the forces and the continuity of the energy flux at the solid surface:

$$\bar{u}\bar{F}_1^{(d)} + \bar{\tau}_w\bar{F}_1^{(1)} = 0, \tag{44}$$

$$\bar{u}\bar{Q}_r^{(d)} + \bar{\tau}_w\bar{Q}_r^{(1)} = -\left.\frac{\lambda_p}{\lambda_{\mathrm{LB}}}\partial_r\tau_{p,1}\right|_{r=1}, \tag{45}$$

where λ_p is the thermal conductivity of the solid and $\lambda_{\mathrm{LB}}T_0=p_0 L\sqrt{2RT_0}$. When the solid sphere undergoes light irradiation, the temperature distribution τ_p follows the diffusion equation in the following form:

$$\nabla^2\tau_p = -\alpha IB/(\lambda_p T_0), \tag{46}$$

where $\alpha=4\pi nk/\lambda$ is an adsorption coefficient, $\tilde{n}=n+ik$ is a complex refraction index, λ is the wavelength of an incident

beam, I is the light intensity, and $B(\boldsymbol{x})$ is the relative power distribution of the electromagnetic field in the sphere. As is known, a general solution of Eq. (46) in a spherical system with a rotational symmetry can be given in the form $\tau_p = \Sigma_n \tau_{p,n} P_n(\cos\theta)$, where $P_n(x)$ is a Legendre polynomial. When we describe $B(\boldsymbol{x})$ with an expansion form as $\Sigma_n B_n(r) P_n(\cos\theta)$, we can derive the following relation:

$$\partial_r \tau_{p,1}|_{r=1} = \tau_{p,1}(1) + \frac{\alpha I}{\lambda_p T_0} \int_0^1 s^3 B_1(s) ds. \tag{47}$$

The photophoretic velocity of the solid particle is obtained in the following form:

$$\bar{u} = \frac{\alpha I \left(\int_0^1 s^3 B_1(s) ds \right) \bar{F}_1^{(1)} / \bar{F}_1^{(d)}}{\lambda_p T_0 + \lambda_{\mathrm{LB}} T_0 (\bar{Q}_r^{(1)} - \bar{Q}_r^{(d)} \bar{F}_1^{(1)} / \bar{F}_1^{(d)})}, \tag{48}$$

where the integral $\int_0^1 s^3 B_1(s) ds$ is equivalent to the asymmetric factor J introduced by Yalamov [21]. Consequently, the migration velocity depends linearly on the laser power as long as the velocity and the temperature difference are small compared with their reference values (the thermal molecular velocity $\sqrt{2RT_0}$ and the gas temperature at infinity T_0).

IV. PHOTOPHORESIS OF A LIQUID SPHERE WITH SLOW INTERNAL FLOW

When an aerosol particle is not solid, the boundary on the particle side may have a nonzero velocity. As shown later, the flow velocity of the first order at the boundary of a spherical liquid droplet linearly depends on $\sin\theta$. When there is no mass flow across the boundary, the velocity distribution function of the ambient gas is given by

$$\phi = \bar{u}\phi_d + \bar{\tau}_w \phi_1 + \bar{u}_w \phi_v, \tag{49}$$

where $\bar{u}_w$ is the magnitude of the flow velocity at the boundary surface of the droplet. The boundary equations in this case are

$$\bar{u}\bar{F}_1^{(d)} + \bar{\tau}_w \bar{F}_1^{(1)} + \bar{u}_w \bar{F}_1^{(v)} = 0, \tag{50}$$

$$\bar{u}\bar{P}_{r\theta}^{(d)} + \bar{\tau}_w \bar{P}_{r\theta}^{(1)} + \bar{u}_w \bar{P}_{r\theta}^{(v)} = \check{P}_{r\theta} - \frac{T_0}{L p_0} \frac{d\gamma}{dT} \tau_w, \tag{51}$$

$$\bar{u}\bar{Q}_r^{(d)} + \bar{\tau}_w \bar{Q}_r^{(1)} + \bar{u}_w \bar{Q}_r^{(v)} = -\left. \frac{\lambda_p}{\lambda_{\mathrm{LB}}} \partial_r \tau_{p,1} \right|_{r=1}, \tag{52}$$

where $p_0 \check{P}_{r\theta} \sin\theta$ is the $r-\theta$ component of a viscous stress tensor at the boundary surface of the droplet and γ is the surface tension of the droplet.

For a liquid droplet, its temperature distribution and the internal flow velocity in a steady state are determined by the Navier-Stokes equations. The nondimensional forms of these equations are given by

$$\nabla \cdot \boldsymbol{u} = 0, \tag{53}$$

$$\mathrm{Re}(\boldsymbol{u} \cdot \nabla)\boldsymbol{u} = -(\nabla p') + \bar{u}_w \nabla^2 \boldsymbol{u}, \tag{54}$$

$$\mathrm{Re}(\boldsymbol{u} \cdot \nabla)\tau = \mathrm{Pr}^{-1} \bar{u}_w (\nabla^2 \tau + \alpha I B / \lambda_p T_0) + \mathrm{Ma}^2 \bar{u}_w^{-1} (\partial_j u_i + \partial_i u_j) \partial_i u_j, \tag{55}$$

where Re is the Reynolds number, Pr is the Prandtl number, Ma is the Mach number, and $\bar{u}_w = U_w / (2RT_0)^{1/2}$ is a dimensionless characteristic velocity. Boundary conditions are given by Eqs. (51) and (52), and the condition of no mass flow across the boundary ($u_r = 0$ at $r=1$). In the above equations, the reference velocity is $\sqrt{2RT_0}$ to match the dimensionless expression of the Boltzmann equation. If we introduce a reference Reynolds number $\mathrm{Re}' = L\sqrt{2RT_0}/\nu$, where ν is a dynamic viscosity coefficient, the Reynolds number is expressed as $\mathrm{Re} = \mathrm{Re}' \bar{u}_w$. Usually, the Mach number (the ratio of the characteristic velocity to the speed of sound) is much smaller than unity, and thus the last term of Eq. (55) (the viscous dissipation function) is negligible. Moreover, we consider here the case in which the Reynolds number Re and the Peclet number Pe($\mathrm{Pe} = \mathrm{Re} \cdot \mathrm{Pr}$) are sufficiently small so that the advective terms in Eqs. (54) and (55) may also be ignored.

In an incompressible fluid [where Eq. (53) holds true], the flow velocity field is determined independently of the temperature field, except for the boundary condition. Equations (53) and (54) can be transformed into the so-called Helmholtz's vorticity equation [47] in terms of the vorticity $\boldsymbol{\omega} = \nabla \times \boldsymbol{u}$. In a spherical system with rotational symmetry in the ϕ direction and with no rotational component of the flow velocity, the vorticity $\boldsymbol{\omega}$ only has a rotational component ω_ϕ. When the advective term is negligible, a general solution for ω_ϕ is given by

$$\omega_\phi = \sum_{n=1}^{\infty} (A_n r^n + B_n r^{-n-1}) P_n^1(\cos\theta), \tag{56}$$

where $P_n^m(\cos\theta)$ is an associated Legendre function. From the definition of vorticity, u_θ and $\partial_\theta u_r$ have expansion forms with respect to $P_n^1(\cos\theta)$. This leads to

$$u_r = a_r^0(r) + \sum_{n=1}^{\infty} a_r^n(r) P_n(\cos\theta), \tag{57}$$

$$u_\theta = \sum_{n=1}^{\infty} a_\theta^n(r) P_n^1(\cos\theta). \tag{58}$$

From Eqs. (53), (57), and (58),

$$a_r^0 = c_0 r^{-2}, \tag{59}$$

and for $n \geq 1$,

$$a_r^n = c_{n1} r^{n+1} + c_{n2} r^{-n} + c_{n3} r^{n-1} + c_{n4} r^{-n-2}, \tag{60}$$

$$a_\theta^n = -\frac{n+3}{n(n+1)} c_{n1} r^{n+1} + \frac{n-2}{n(n+1)} c_{n2} r^{-n} - \frac{1}{n} c_{n3} r^{n-1} + \frac{1}{n+1} c_{n4} r^{-n-2}. \tag{61}$$

Since there is no flow across the boundary, we obtain the following solution for the mode $n=1$:

$$u_r = \bar{u}_w(1-r^2)\cos\theta, \tag{62}$$

$$u_\theta = \bar{u}_w(-1+2r^2)\sin\theta. \tag{63}$$

For this flow field, the $r-\theta$ component of the viscous stress tensor at $r=1$ takes the form

$$\check{P}_{r\theta} = -6\,\mathrm{Re}'^{-1}(\rho_p/\rho_0)\bar{u}_w. \tag{64}$$

On the other hand, since the Peclet number is assumed to be small, the temperature field follows a simple diffusion equation. In this case, the gradient of the temperature at $r=1$ follows Eq. (47) in the preceding section. Thus, the photophoretic velocity is derived to show linear dependence on the laser power as follows:

$$\bar{u} = \frac{-\alpha I\int s^3 B_1(s)ds/(\lambda_{\mathrm{LB}}T_0)}{Q_r^{(d)} + Q_r^{(v)}\dfrac{\bar{F}_1^{(1)}\bar{P}_{r\theta}^{(d)} - \bar{F}_1^{(d)}\bar{P}_{r\theta}^{(1)\prime}}{\bar{F}_1^{(v)}\bar{P}_{r\theta}^{(1)\prime} - \bar{F}_1^{(1)}\bar{P}_{r\theta}^{(v)\prime}} + \bar{Q}_r^{(1)\prime}\dfrac{\bar{F}_1^{(d)}\bar{P}_{r\theta}^{(v)\prime} - \bar{F}_1^{(v)}\bar{P}_{r\theta}^{(d)}}{\bar{F}_1^{(v)}\bar{P}_{r\theta}^{(1)\prime} - \bar{F}_1^{(1)}\bar{P}_{r\theta}^{(v)\prime}}}, \tag{65}$$

where $\bar{Q}_r^{(1)\prime} = \bar{Q}_r^{(1)} + \lambda_p/\lambda_{\mathrm{LB}}$, $\bar{P}_{r\theta}^{(v)\prime} = \bar{P}_{r\theta}^{(v)} + 6\,\mathrm{Re}'^{-1}(\rho_p/\rho_0)$, and $\bar{P}_{r\theta}^{(1)\prime} = \bar{P}_{r\theta}^{(1)} + T_0(d\gamma/dT)/(Lp_0)$.

V. PHOTOPHORESIS OF A LIQUID SPHERE WITH MODERATELY FAST INTERNAL FLOW

When the Peclet number is not small, the advective term in the energy equation is not negligible. In this case, the detailed structure of the relative power distribution becomes important. Later in this section, we introduce a parameter B_{mn}. To avoid confusing the notation with B_n, we briefly summarize these notations:

$$B(\boldsymbol{x}) = B_n(r)P_n(\cos\theta) = B_{mn}\hat{B}_{mn}(r,\theta), \tag{66}$$

where $\hat{B}_{mn}(r,\theta) = r^n P_m(1-2r)P_n(\cos\theta)$. When $B(\boldsymbol{x})$ is given, B_{mn} is calculated as follows:

$$B_{mn} = \frac{(2m+1)(2n+1)}{4\pi}\int_0^{2\pi}\int_{-1}^{1}\int_0^1 B(\boldsymbol{x})r^{-n} \times P_m(1-2r)P_n(\cos\theta)drd\cos\theta d\phi. \tag{67}$$

Hereafter, we consider the case where the Reynolds number is small ($0<\mathrm{Re}<1$), but the Peclet number is not necessarily small ($0<\mathrm{Pe}<\mathrm{Pr}$, $\mathrm{Pr}\gg 1$). Thus, the flow in the droplet is represented by Eqs. (62) and (63), and the energy equation is described as

$$\sum_n\left[(1-r^2)\partial_r\tau_n\left(\frac{n+1}{2n+1}P_{n+1}(\cos\theta)+\frac{n}{2n+1}P_{n-1}(\cos\theta)\right)+\frac{2r^2-1}{r}\tau_n\left(\frac{n(n+1)}{2n+1}P_{n+1}(\cos\theta)-\frac{n(n+1)}{2n+1}P_{n-1}(\cos\theta)\right)\right.$$
$$\left.-\mathrm{Pe}^{-1}\left(\frac{1}{r^2}\partial_r(r^2\partial_r\tau_n)P_n(\cos\theta)-\frac{n(n+1)}{r^2}\tau_n P_n(\cos\theta)+\frac{\alpha I}{\lambda_p T_0}B_n(r)P_n(\cos\theta)\right)\right]=0. \tag{69}$$

Since $P_n(\cos\theta)$ are orthogonal, each coefficient for $P_n(\cos\theta)$ must be 0;

$$(1-r^2)\left(\frac{n}{2n-1}\partial_r\tau_{n-1}+\frac{n+1}{2n+3}\partial_r\tau_{n+1}\right)+\frac{2r^2-1}{r}\left(\frac{n(n-1)}{2n-1}\tau_{n-1}-\frac{(n+1)(n+2)}{2n+3}\tau_{n+1}\right)$$
$$-\mathrm{Pe}^{-1}\left(\frac{1}{r^2}\partial_r(r^2\partial_r\tau_n)-\frac{n(n+1)}{r^2}\tau_n+\frac{\alpha I}{\lambda_p T_0}B_n(r)\right)=0. \tag{70}$$

Equation (70) is singular at $r=0$. Roughly, the advective term is on the order of τ/r and the diffusion term is on the order of τ/r^2. Thus, in the limit of $r\to 0$, diffusion should determine the leading term of the solution. The general solution of the diffusion equation takes the form $\tau_n = C_1 r^n + C_2 r^{-n-1}$. Since we are only interested in a finite solution, the leading term of τ_n scales as r^n in the limit $r\to 0$. Thus, when we consider the solution in the form $\tau_n(r) = r^n\tau_n'(r)$, the function τ_n' does not

diverge in the limit $r \to 0$. Equation (70) can be rewritten in terms of τ_n' as follows:

$$\partial_r^2 \tau_n' = -\bar{I} b_n(r) - 2(n+1) r^{-1} \partial_r \tau_n' + \mathrm{Pe}\left[\frac{n}{2n-1} \frac{1-r^2}{r} \partial_r \tau_{n-1}' + \frac{n+1}{2n+3} r(1-r^2) \partial_r \tau_{n+1}' + \frac{n(n-1)}{2n-1} \tau_{n-1}' - \frac{(n+1)(n+2)}{2n+3} r^2 \tau_{n+1}' + (n+1)(1-r^2) \tau_{n+1}' \right], \quad (71)$$

where $r^n b_n(r) = B_n(r)$ and $\bar{I} = \alpha I / (\lambda_p T_0)$.

For $n=0$, the following relation is derived from the above equation:

$$\partial_r \tau_0' = -\frac{\bar{I}}{r^2} \int_0^r s^2 b_0(s) ds + \frac{\mathrm{Pe}}{3} (r - r^3) \tau_1'. \quad (72)$$

If we omit a contribution from τ_2', Eq. (71) for $n=1$ and Eq. (72) lead to a dominant equation for τ_1':

$$\partial_r (r^4 \partial_r \tau_1') - \frac{\mathrm{Pe}^2}{3} r^4 (1-r^2)^2 \tau_1' + f(r) = 0, \quad (73)$$

$$f(r) = \bar{I} r^4 b_1(r) + \bar{I}\, \mathrm{Pe}\, r(1-r^2) \int_0^r s^2 b_0(s) ds. \quad (74)$$

From Eqs. (50) and (51) with Eq. (64), we can easily determine that $\bar{u}$, $\bar{\tau}_w$, and $\bar{u}_w$ are linearly dependent on each other. Here, we express $\bar{u}$ and $\bar{u}_w$ with $\bar{\tau}_w$;

$$\bar{u} = \xi_u \bar{\tau}_w, \quad (75)$$

$$\bar{u}_w = \xi_{uw} \bar{\tau}_w. \quad (76)$$

By substituting Eqs. (75) and (76) into Eq. (52), we obtain the first boundary condition

$$(\bar{\xi} + 1) \tau_1'(1) + \partial_r \tau_1'(1) = 0. \quad (77)$$

For $r=0$, $\partial_r \tau_n'$ must be 0. Otherwise, the energy equation [Eq. (71)] becomes singular at $r=0$. This is the second boundary condition

$$\partial_r \tau_1'(0) = 0. \quad (78)$$

[Notably, $\lim_{r \to 0} (\partial_r \tau_n')/r$ is not necessarily 0. Thus, the actual boundary condition at $r=0$ is given by the continuity of $\partial_r^2 \tau_n'$.]

Equation (73) has one undetermined parameter Pe, and we need an additional condition to determine it. Since the Peclet number $\mathrm{Pe} = \mathrm{Pr} \cdot \mathrm{Re}'\, \bar{u}_w$, Eq. (76) leads to

$$\tau_1(1) = \xi_{\mathrm{sur}}\, \mathrm{Pe}. \quad (79)$$

To find a general trend of the solution, it is convenient to calculate the Green's function $G_{\mathrm{Pe}}(r, r')$ for Eq. (73) with the boundary conditions [Eqs. (77) and (78)]. Once the Green's function is solved, the temperature distribution at $r=1$ is given by

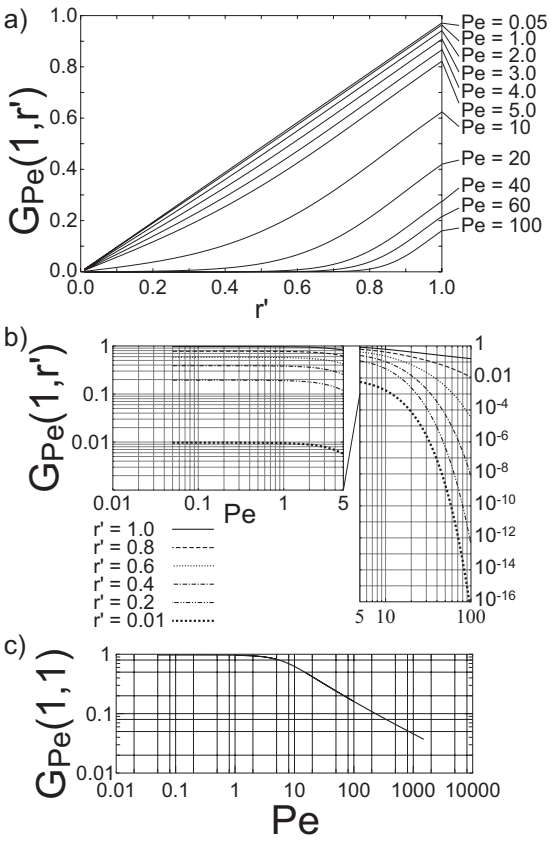

FIG. 2. (a) Green's functions of the surface temperature for various Peclet numbers versus the radial distance in the droplet. (b) The Green's functions at various r's versus the Peclet number. (c) The Green's function at r' versus the Peclet number over a wide range.

$$\tau_1(1) = \int_0^1 G_{\mathrm{Pe}}(1, r') f(r') dr'. \quad (80)$$

If we consider the right-hand side of Eq. (80) as a function of the Peclet number, the Peclet number (and consequently the migration velocity $-\bar{u}$) would be determined as an intersection of the two curves of Eqs. (79) and (80). Unfortunately, it is difficult to derive the analytic expression of $G_{\mathrm{Pe}}(1, r')$, and we must solve it numerically. For a water droplet of 1.0 μm in radius suspended in air with Knudsen number $k=0.1$ (corresponding to 6.0×10^4 Pa) at room temperature (25 °C), the coefficients of the equations can be calculated as $\bar{\xi} = 0.029$ and $\xi_{\mathrm{sur}} = 8.6 \times 10^{-3}$. Water is just an example for assigning numerical values to the parameters, and we expect that a general trend of the solution is not influenced by the specific values of the parameters. However, for a droplet of water, the present analysis is justified only for a Peclet number less than, roughly, 10. Beyond this region, the Reynolds number is larger than 1, and a more careful analysis for the advective term $(\boldsymbol{u} \cdot \nabla)\boldsymbol{u}$ is required.

Figure 2(a) shows a plot of the Green's function $G_{\mathrm{Pe}}(1, r')$ for this case for various values of the Peclet number, ranging from Pe=0.05 to Pe=100. For a small Peclet number, the Green's function is almost linear with respect to the radial

distance. This situation corresponds to the case where the advective term is negligible, which is discussed in the previous section. When the Peclet number exceeds Pe=1, the Green's function starts to noticeably stray from a diffusion-dominant line. Figure 2(b) shows the dependence of the Green's function at each point on the Peclet number as a double-logarithmic plot. The slopes of the curves decrease as the Peclet number increases. When the Peclet number is Pe =5, the Green's function near the center of the droplet decreases as $\mathrm{Pe}^{-\alpha}$ with $\alpha \approx 1$. In this region, the value for α depends on the radial distance r', but this dependency is not extreme. Consequently, the relation among the surface temperature variation $\bar{\tau}_w$, the Peclet number Pe and the radiation power I can be estimated from the representative radial distance (and the corresponding α) where $G_{\mathrm{Pe}}(1,r')f(r')$ has a maximum weight. When the contribution from the B_0 component of the power distribution is dominant,

$$\bar{\tau}_w \sim \mathrm{Pe} \sim I\ \mathrm{Pe}\ G_{\mathrm{Pe}}, \tag{81}$$

and $\bar{\tau}_w$ has a quasiscaling relation as $\bar{\tau}_w = I^{1/\alpha}$. When the contribution from the B_1 component is dominant,

$$\bar{\tau}_w \sim \mathrm{Pe} \sim I G_{\mathrm{Pe}}, \tag{82}$$

and $\bar{\tau}_w$ has an interim scaling relation $\bar{\tau}_w = I^{1/(1+\alpha)}$. Thus, when the B_1 component is dominant and has a particular weight near the center of the droplet, the temperature difference $\bar{\tau}_w$ and consequently the photophoretic velocity $\bar{u}$ exhibit an interim scaling relation with the radiation power as $\bar{u} \sim I^{1/2}$ within a narrow range near Pe=5. However, in a general sense, there is no power law in this intermediate range of the Peclet number.

On the other hand, for a large Peclet number the photophoretic velocity shows a power law. From the curves for $\mathrm{Pe} \geq 20$ in Fig. 2(a), each Green's function can be approximated with a hinge-shaped line. In fact, for the corresponding Peclet number in Fig. 2(b), the Green's function near the center of the droplet falls off very rapidly, while that on the surface $G_{\mathrm{Pe}}(1,1)$ decreases moderately. Thus, we can approximate the Green's function for a large Peclet number as

$$G_{\mathrm{Pe}}(1,r') \simeq \begin{cases} 0 & \text{if } r' < 1 - hG_{\mathrm{Pe}}(1,1) \\ G_{\mathrm{Pe}}(1,1) + (r-1)/h & \text{if } r' > 1 - hG_{\mathrm{Pe}}(1,1), \end{cases} \tag{83}$$

where h is the inverse of $\partial G_{\mathrm{Pe}}(1,r')/\partial r'$ at $r'=1$. To be precise, h is given by

$$h = 1 + \bar{\xi}\tau_{1a}(1)/\dot{\tau}_{1a}(1), \tag{84}$$

where $\tau_{1a}(r)$ is the solution of the homogeneous equation for Eq. (73), which satisfies the boundary condition [Eq. (78)] and $\dot{\tau}_{1a}(r)$ is its derivative. Since $\bar{\xi} \ll 1$, h can be approximated as $h \approx 1$.

When the Peclet number is large and the radiation power distribution changes only moderately near the surface, the surface temperature can be expressed as the following first-order approximation:

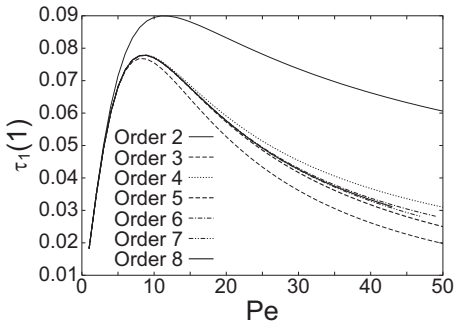

FIG. 3. The τ_1 component of the surface temperature under a homogeneous radiation intensity versus the Peclet number. The lines are solutions of systems of ordinary differential equations transformed from the thermal advective equation, up to the second, third,…, and eighth orders, respectively.

$$\bar{\tau}_w \simeq \frac{\alpha I}{\lambda_p T_0}\left[\frac{1}{3}\mathrm{Pe}\ G_{\mathrm{Pe}}(1,1)^3 \int_0^1 s^2 B_0(s)ds + \frac{1}{2}G_{\mathrm{Pe}}(1,1)^2 B_1(1)\right]. \tag{85}$$

Thus, when $G_{\mathrm{Pe}}(1,1) \sim \mathrm{Pe}^{-\alpha}$, the photophoretic velocity scales as $\bar{u} \sim I^{1/(3\alpha)}$ for the case where the B_0 component is dominant, and as $\bar{u} \sim I^{1/(1+2\alpha)}$ for the case where the B_1 component is dominant. Since the ratio of the contribution from the B_0 component to that from the B_1 component scales to $G_{\mathrm{Pe}}(1,1)\mathrm{Pe}$, in the limit $\mathrm{Pe} \to \infty$ the photophoretic velocity should scale as $\bar{u} \sim I^{1/(3\alpha)}$ unless α is larger than 1.

Figure 2(c) shows a plot of the Green's function $G_{\mathrm{Pe}}(1,1)$ for a wider range of the Peclet number. In this figure, we can clearly distinguish two regions with different scaling relations. One is the diffusion-dominant region for $\mathrm{Pe} < 1$ and the other is the highly advective region for $\mathrm{Pe} > 20$. For the latter case, at least up to Pe=1500, the Green's function $G_{\mathrm{Pe}}(1,1)$ numerically scales as $G_{\mathrm{Pe}}(1,1) \sim \mathrm{Pe}^{-\alpha}$ with an almost constant α of 0.57. Thus, the photophoretic velocity scales as $\bar{u} \sim I^{0.58}$ for the case where the B_0 component is dominant, and as $\bar{u} \sim I^{0.47}$ for the case where the B_1 component is dominant.

The approximation to retain up to the τ_1 component in the ordinary differential system for a thermal transport system discussed above is a very rough version of the spectral method [48] for a (partial) differential system. Though this rough case is numerically stable, and is advantageous for directly calculating the Green's function on real space, it is not very accurate. Figure 3 shows a plot of the numerical solutions of $\tau_1(1)$ with a homogeneous radiation intensity $[B_0(r)=1]$, while varying the fineness of the spectral method. The term "order n" means that, up to τ_n, the components of the differential equations are retained. This figure shows that the second-order approximation only reproduces the qualitative behavior. On the other hand, the numerical solutions for higher-order approximations can only be obtained in a limited range of the Peclet number.

As described above, for a higher-order approximation, the Green's function on real space is not calculated directly. On

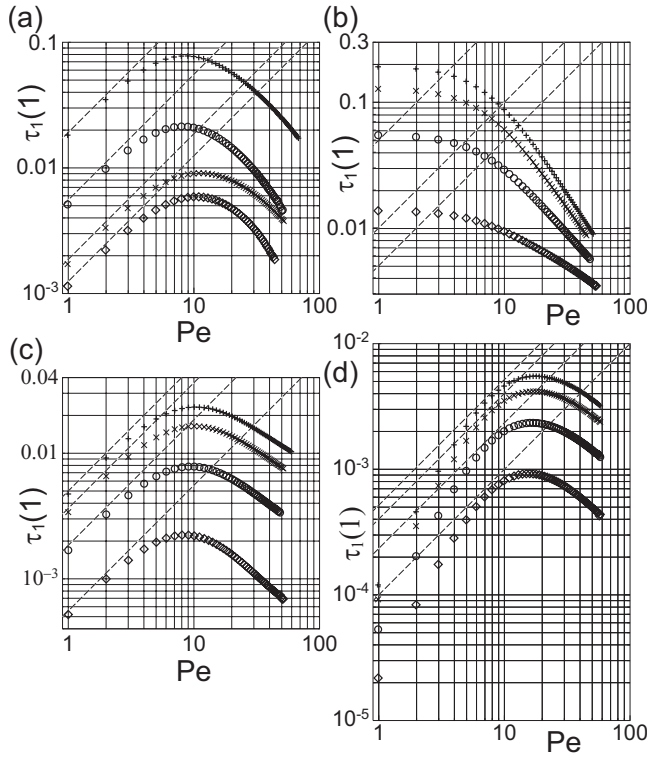

FIG. 4. The τ_1 component of the surface temperature versus the Peclet number under a radiation intensity distribution in the form of various base functions as $\hat{B}_{mn}(r,\theta)=r^n P_m(1-2r)P_n(\cos\theta)$ where $n=0$ for (a), $n=1$ for (b), $n=2$ for (c), and $n=3$ for (d). The symbols, +, ×, ○, and ◇, in the figure correspond to $m=0$, $m=1$, $m=2$, and $m=3$, respectively. Thin dashed lines were introduced as auxiliary lines to show the slope of the line of the boundary condition, $\tau_1 \sim \mathrm{Pe}$.

the other hand, since the delta function is regarded as an infinite summation of eigenfunctions, the Green's function can be constructed as an infinite summation of response functions for each base function. If we change our viewpoint, the set of these response functions can be substituted for the Green's function. Figure 4 shows a plot of $\tau_1(1)$ versus the Peclet number for various base functions in the form of $\hat{B}_{mn}(r,\theta)=r^n P_m(1-2r)P_n(\cos\theta)$, where $P_n(x)$ is a Legendre polynomial. Thin dashed lines in the figure were introduced to show the slope of the line of the boundary condition [Eq. (79)]. To be exact, the line of the boundary condition exists uniquely, and the curves of the response functions shift upward as the radiation intensity increases. In principle, this is equivalent to considering that the line of the boundary condition shifts downward as the radiation intensity increases, as long as the Peclet number at a steady state is considered. The actual steady state is the intersection of the line of the boundary condition with the total response function according to the actual radiation distribution structure, but its general behavior can be estimated from the intersections with individual radiation modes.

As shown in Fig. 4, the scaling behavior differs according to the base function of the radiation intensity distribution. With regard to τ_1, the advection-dominant region first appears for the base function of $n=1$. For $n=1$, the magnitude of the scaling exponent of τ_1 against Pe is largest for $m=0$, and decreases as the value of m increases. This tendency is specific to $n=1$, and for a larger value of n, the opposite trend is seen. However, in the case of $n=3$, the advection-dominant region is not sufficiently calculated, and it is difficult to make a clear conclusion at present. For $n=0$, the horizontal position of each curve is not regular. From top to bottom, the curves are, respectively, for $m=0$, $m=2$, $m=1$, and $m=3$, respectively. This irregular behavior can be attributed to the total energy flux acting on the droplet. For $n=0$, the total energy inflow scales to $\int_0^1 s^2 P_m(1-2s)ds$, and this term can be rewritten by using $P_m^*(s)=P_m(1-2s)$ as follows:

$$\int_0^1 s^2 P_m^*(s)ds = \int_0^1 \left(\frac{1}{6}P_2^*(s) - \frac{1}{2}P_1^*(s) + \frac{1}{3}P_0^*(s)\right)P_m^*(s)ds. \tag{86}$$

From the above expression, it is clear that the total energy inflow is 1/3 for $m=0$, $-1/6$ for $m=1$, and 1/30 for $m=2$. For $m\leq 3$ or $n\leq 1$, the total energy inflow is 0. Consequently, $\tau_1(1)$ shows a regular behavior for these modes of the radiation intensity distribution.

Overall, the response of $\tau_1(1)$ is largest for $n=1$ and $m=0$ and decreases as $|n-1|$ and/or m increase. In principle, the intensity distribution in a spherical dielectric under irradiation with a planar wave can be given by the Mie solution [26,27]. According to the ratio of diameter to wavelength, the behavior of the Mie solution can be analyzed for three cases. In one case, the diameter of the dielectric is much larger than the wavelength of the incident beam, and the dielectric can be considered a spherical lens. In this case, the dominant modes of the intensity distribution would be B_{00} and B_{01}. Thus, the scaling of the photophoretic velocity to the radiation intensity is determined by the ratio B_{01}/B_{00} and the absolute value of the radiation intensity. In Fig. 4, the steady state is roughly determined by the highest of the intersections of each curve with the line of the boundary condition [Eq. (79)]. The absolute value of the radiation intensity shifts the temperature level for all curves. When the intensity I goes to 0, all curves in the figure shift downward infinitely. For a sufficiently small I, the line of the boundary condition first meets the solution for B_{01} with a very small Peclet number. In this region, the solution for B_{m1} shows a flat profile, and the intersection follows a scaling relation $I \sim \xi_{\mathrm{sur}}\,\mathrm{Pe}$.

When I becomes large, the Peclet number at the intersection becomes large and the contribution from B_{00} becomes large. In particular, for the case in which B_{01}/B_{00} is much smaller than 1, the solution for B_{00} is a dominant contribution to τ_1. After the intersection passes the peak of the solution, the intersection numerically follows a scaling relation $I\,\mathrm{Pe}^{-1.2} \sim \xi_{\mathrm{sur}}\,\mathrm{Pe}$. Consequently, the photophoretic velocity scales to $I^{0.45}$. If the ratio B_{01}/B_{00} is not small, the dominant contribution is the solution for B_{01}. In this case, the intersection numerically follows a scaling relation $I\,\mathrm{Pe}^{-1.5} \sim \xi_{\mathrm{sur}}\,\mathrm{Pe}$, and the photophoretic velocity scales to $I^{0.4}$. These scaling exponents are slightly smaller than the earlier rough estimations based on the two-mode approximation. On the other hand, solutions for B_{m0} do not seem to sufficiently reach an

asymptotic region within the calculated range. From the wide-range calculations for the two-mode approximation shown in Fig. 2(c), we can be certain that solutions for B_{m0} would exhibit an asymptotic scaling behavior for a large value of the Peclet number. However, the actual asymptotic scaling exponent may shift from the above discussed value.

Interestingly, in Fig. 4(d), a curve for B_{m3} sometimes has two intersections with the line of the boundary condition. The smaller intersection corresponds to an unstable steady state. This behavior is not seen in the other modes. Due to the essential property of the system, in the limit of a small Peclet number, the response functions for the B_{m0} and B_{m2} modes would show asymptotic linear scaling. The response functions for the B_{m1} modes would show an asymptotic constant behavior. This difference depends on how many times the internal flow acts to produce a τ_1 temperature distribution. For the B_{m3} modes, the internal flow acts twice, and thus the response function has an asymptotic scaling relation as $\tau_1 \sim \mathrm{Pe}^2$ for a small Peclet number. Consequently, for the B_{m3} modes or modes of higher order than B_{m3}, there is a threshold of the photophoretic velocity. For the B_{m0} and B_{m2} modes, while there is no threshold of the photophoretic velocity, there is a threshold of the intensity to induce photophoresis.

Variation in size influences the photophoretic velocity by changing the boundary parameters (ξ_u, ξ_{uw}, $\bar{\xi}$, and ξ_{sur}) and by changing the heat source function. The formula for the heat source function is established but rather complicated, which depends on the wave length, the complex refraction index and the size of sphere itself. To understand a general trend of the effect of thermodynamic processes, we focus on the changes in ξ_u, ξ_{uw}, $\bar{\xi}$, and ξ_{sur}.

The parameter $\bar{\xi}$ represents the magnitude of the heat flow from the droplet to the gas. Since λ_{LB} scales to the size of droplet L, $\bar{\xi}$ increases linearly to the increase in L, unless the other parameters do not change. In fact, when L increases under the same pressure, the Knudsen number k decreases and the value of $\bar{\xi}$ changes in a more complicated manner. However, $\bar{\xi}$ basically increases with the increase in L. It is interesting that this change in $\bar{\xi}$ only slightly changes the Green's function. In addition, ξ_{uw} does not change very much with the change in L.

The parameter ξ_{sur} is a ratio of the surface temperature difference to the Peclet number, and it decreases with the increase in L. When ξ_{sur} decreases, the solution for the Peclet number increases. Finally, ξ_u associates the Peclet number with the photophoretic velocity $-U$;

$$\frac{\mathrm{Pe}\ \xi_u}{L\xi_{uw}} = U\ \mathrm{Pr}/\nu. \tag{87}$$

In principle, the photophoretic velocity decreases as L increases because ξ_u decreases.

Figure 5 is the plot of $\mathrm{Pe}\ \xi_u/(L\xi_{uw})$ versus L for various values of $\bar{I}B_{01}$ and $\bar{I}B_{00}$. For $\bar{I}B_{00}$=0.01, there is no photophoresis. It is notable that U changes its sign from the positive to the negative when L increases. This fact is characteristic to a liquid droplet (of which surface tension decreases as

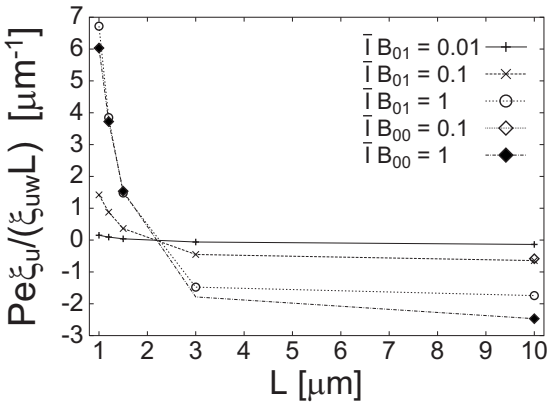

FIG. 5. The size dependence of the photophoretic velocity. $\mathrm{Pe}\ \xi_u/(\xi_{uw}L)$ is equivalent to $U\ \mathrm{Pr}/\nu$, where $-U$ corresponds to the photophoretic velocity.

the temperature increases). For a solid particle, photophoretic velocity falls off to zero as L increases. The negative value of U means the photophoretic motion toward the heated side. In this case, the droplet swims because of the Marangoni convection. The sign of U depends on the size of the droplet L but is independent of the radiation intensity $\bar{I}$.

In principle, inhomogeneous surface tension induces not only the convection but also the deformation of the droplet. While the convection is determined by the space derivative of surface tension, the deformation is determined by the surface tension itself. Let us consider droplets in different sizes with the same surface temperature distribution in angle. The convection becomes more rapid as the size of the droplet decreases. On the other hand, the deformation of the droplet is independent of the size of the droplet. Thus, for a small droplet, the deformation is not significant as compared with the convection. Usually, the deformation is taken into account for a centimeter-sized droplet.

For a symmetrical model system, photophoretic motion occurs along a light axis. In fact, in many actual experiments, the photophoretic force pointed toward the direction of a light axis. However, the photophoresis of a different type is also observed [12]. At present, such anomalous photophoresis is associated with inhomogeneity of the photophoretic particle. For example, when the particle surface is not clean, the accommodation coefficient is occasionally position dependent. In this case, the photophoretic force (called the $\Delta\alpha$ force [11]) arises as a body-fixed force and the particle moves toward a direction independent of the light axis. Inhomogeneity can also influence the temperature distribution. When a spheroid is illuminated from an oblique direction, the direction of the photophoretic force can theoretically deviate from the light axis [29]. In these explanations, anomalous photophoresis is characteristic to a solid particle. Since the B_{m0} mode of the radiation distribution has no particular direction, it is clear that an internal flow or temperature field sustained by this homogeneous mode does not depend on the direction of the light axis. In this case, the direction of the photophoresis would be easily influenced by fluctuations and disturbances of the system. Thus, the present result suggests that anomalous photophoresis can occur for a liquid droplet

due to the coupling of a homogeneous energy inflow and an internal flow field.

A nonlinear scaling relation between photophoretic force and radiation intensity was also discussed by Sitarski [32]. In his model, the Stefan-Boltzmann law of blackbody radiation (T^4 dependence) and evaporation increasing exponentially to T were the main causes of nonlinearity. Nonlinearity basically originates from the boundary condition, and this situation is similar to the present analysis. Whether or not blackbody radiation is negligible depends on thermodynamic variables. Let us consider dried air at 10^5 Pa and 300 K. If a temperature difference in the system is on the order of 5 K and the Knudsen number is $k=0.1$, the dimensionless heat flow originating from problem 2 is on the order of 2×10^{-3}. On the other hand, the dimensionless heat flow between 305 K blackbody and 300 K background radiation field is on the order of 10^{-6}. In this case, the effect of heat radiation is actually negligible. It is notable that heat radiation is independent of the pressure if the gas is transparent, but the heat flow arising from molecular collisions highly depends on the pressure. In a nonvacuum condition, heat radiation is negligible as a matter of fact. In a medium-vacuum condition, these two terms can be comparable. In a high-vacuum condition, heat radiation can be the main influence on the temperature distribution. The effect of evaporation highly depends on the material. To explain the photophoresis of a volatile oil droplet, this effect must be considered correctly. The present discussion should also promote our understanding of the essential physics of this problem.

VI. CONCLUSION

The photophoresis of a microdroplet is discussed with Navier-Stokes equations for a liquid region coupled with the linearized Boltzmann equation for a gaseous region. When internal flow is slow, a temperature distribution inside the droplet is determined by the diffusion equation. In this case, the photophoretic velocity linearly scales to the radiation intensity. Only difference with the case of a solid sphere is its coefficient. When internal flow is fast, the temperature advection changes the behavior of the system in a qualitative manner. We observed an asymmetric flow field induced by a homogeneous mode of the radiation intensity distribution inside the droplet. While such a mixing of modes is a characteristic of nonlinear phenomena, this case has a much simpler explanation. A homogeneous mode is not an eigenmode for this system even if the hydrodynamic equation is linearized. On the other hand, since nonlinear coupling exists between the flow field and temperature field through the boundary condition, a nonlinear relation appears between the photophoretic velocity and the radiation intensity. For a sufficiently strong radiation intensity, the photophoretic velocity scales to the intensity with a scaling exponent of about 0.4, and the actual value depends on the intensity distribution inside the droplet. In addition, the radiation intensity can switch the dominant mode of the radiation distribution and a threshold behavior is anticipated for the photophoretic velocity.

[1] I. Simanovskii, A. Nepomnyashchy, V. Shevtsova, P. Colinet, and J.-C. Legros, Phys. Rev. E **73**, 066310 (2006).
[2] N. Tiwari, Z. Mester, and J. M. Davis, Phys. Rev. E **76**, 056306 (2007).
[3] L. Rongy and A. De Wit, Phys. Rev. E **77**, 046310 (2008).
[4] F. Ehrenhaft, Phys. Z. **18**, 352 (1917).
[5] S. G. Warren and W. J. Wiscombe, J. Atmos. Sci. **37**, 2734 (1980).
[6] H. Rosen, T. Novakov, and B. A. Bodhaine, Atmos. Environ. **15**, 1371 (1981).
[7] V. V. Karasev, N. A. Ivanova, A. R. Sadykokova, N. Kukhareva, A. M. Baklanov, A. A. Onischuk, F. D. Kovalev, and S. A. Beresnev, J. Aerosol Sci. **35**, 363 (2004).
[8] V. G. Chernyak and S. A. Beresnev, J. Aerosol Sci. **24**, 857 (1993).
[9] H. B. Lin, Opt. Lett. **10**, 68 (1985).
[10] E. R. Buckle and Y. M. Bushnell-Watson, J. Colloid Interface Sci. **105**, 529 (1985).
[11] G. Wurm and O. Krauss, Atmos. Environ. **42**, 2682 (2008).
[12] O. Jovanovic, J. Quant. Spectrosc. Radiat. Transf. **110**, 889 (2009).
[13] H. Watarai, H. Monjushiro, S. Tsukahara, M. Suwa, and Y. Iiguni, Anal. Sci. **20**, 423 (2004).
[14] T. Imasaka, Y. Kawabata, T. Kaneta, and Y. Ishidzu, Anal. Chem. **67**, 1763 (1995).
[15] T. W. Ng, A. Neild, and P. Heeraman, Opt. Lett. **33**, 584 (2008).
[16] T. X. Phuoc, Opt. Commun. **245**, 27 (2005).
[17] A. Ashkin, Biophys. J. **61**, 569 (1992).
[18] H. Monjushiro, A. Hirai, and H. Watarai, Langmuir **16**, 8539 (2000).
[19] Y. Sone, *Molecular Gas Dynamics: Theory, Techniques, and Applications* (BirkHäuser, Boston, 2007).
[20] N. T. Tong, J. Colloid Interface Sci. **51**, 143 (1975).
[21] Y. I. Yalamov, V. B. Kutukov, and E. R. Shchukin, J. Colloid Interface Sci. **57**, 564 (1976).
[22] L. D. Reed, J. Aerosol Sci. **8**, 123 (1977).
[23] M. Sitarski and M. Kerker, J. Atmos. Sci. **41**, 2250 (1984) and references therein.
[24] P. W. Dusel, M. Kerker, and D. D. Cooke, J. Opt. Soc. Am. **69**, 55 (1979).
[25] D. W. Mackowski, Int. J. Heat Mass Transfer **32**, 843 (1989).
[26] M. Born and E. Wolf, *Principles of Optics*, 7th (expanded) ed. (Cambridge University Press, New York, 1999).
[27] G. Mie, Ann. Phys. **330**, 377, (1908).
[28] Y.-L. Xu, B. Å. S. Gustafson, F. Giovane, J. Blum, and S. Tehranian, Phys. Rev. E **60**, 2347 (1999).
[29] C. L. Ou and H. J. Keh, J. Colloid Interface Sci. **282**, 69 (2005).
[30] C.-Y. Soong, W.-K. Li, C.-H. Liu, and P.-Y. Tzeng, Opt. Lett. **35**, 625 (2010).
[31] C. H. Liu, C. Y. Soong, W. K. Li, and P. Y. Tzeng, J. Quant.

Spectrosc. Radiat. Transf. **111**, 483 (2010).
[32] M. Sitarski, J. Colloid Interface Sci. **105**, 502 (1985).
[33] L. Waldmann, Z. Naturforsch. B **14a**, 589 (1959).
[34] W. F. Phillips, Phys. Fluids **15**, 999 (1972).
[35] F. Zheng, Adv. Colloid Interface Sci. **97**, 253 (2002).
[36] P. S. Epstein, Z. Phys. **54**, 537 (1929).
[37] J. R. Brock, J. Colloid Sci. **17**, 768 (1962).
[38] Y. Sone and K. Aoki, in *Rarefied Gas Dynamics*, edited by J. L. Potter (AIAA, New York, 1977), Vol. 417.
[39] L. Talbot, R. K. Cheng, R. W. Schefer, and D. R. Willis, J. Fluid Mech. **101**, 737 (1980).
[40] Y. Sone and K. Aoki, J. Mec. Theor. Appl. **2**, 3 (1983).
[41] K. Yamamoto and Y. Ishihara, Phys. Fluids **31**, 3618 (1988).
[42] S. K. Loyalka, J. Aerosol Sci. **23**, 291 (1992).
[43] S. Beresnev, V. Chernyak, and G. Fomyagin, Phys. Fluids A **5**, 2043 (1993).
[44] W. Li and E. J. Davis, J. Aerosol Sci. **26**, 1085 (1995).
[45] S. Arnold and M. Lewittes, J. Appl. Phys. **53**, 5314 (1982).
[46] H. Grad, in *Rarefied Gas Dynamics*, edited by J. A. Laurmann (Academic Press, New York, 1963), Vol. 26.
[47] H. Lamb, *Hydrodynamics*, 6th ed. (Dover, New York, 1993).
[48] J. P. Boyd, *Chebyshev and Fourier Spectral Methods* (Dover, New York, 2000).